Applied Physics Express

Enhancement of coercive field in atomically-thin quenched Fe₅GeTe₂

To cite this article before publication: Tomoharu Ohta *et al* 2020 *Appl. Phys. Express* in press https://doi.org/10.35848/1882-0786/ab7f18

Applied Physics Express

Enhancement of coercive field in atomically-thin quenched Fe_5GeTe_2

Tomoharu Ohta[1], Kosuke Sakai[1], Hiroki Taniguchi[1], Benjamin Driesen[2], Yoshinori Okada[2], Kensuke Kobayashi[1,3], and Yasuhiro Niimi[1,4]*

[1] *Department of Physics, Graduate School of Science, Osaka University, Toyonaka, Osaka 560-0043, Japan*
[2] *Okinawa Institute of Science and Technology Graduate University, Okinawa 904-0495, Japan*
[3] *Institute for Physics of Intelligence and Department of Physics, The University of Tokyo, Bunkyo-ku, Tokyo 113-0033, Japan*
[4] *Center for Spintronics Research Network, Osaka University, Toyonaka, Osaka 560-8531, Japan*

We have fabricated thin films of a van der Waals (vdW) ferromagnetic metal Fe_5GeTe_2 and characterized them by measuring the anomalous Hall effect. While the bulk Fe_5GeTe_2 does not exhibit a perpendicular magnetic anisotropy (PMA) unlike Fe_3GeTe_2, PMA emerges in the thin film devices. Furthermore, the PMA is enhanced with decreasing the thickness of Fe_5GeTe_2. In particular, a thin film (5 unit-cell layer) device fabricated with Fe_5GeTe_2 quenched at 1050 K has two times larger coercive field than that prepared without quenching. Such a PMA should be useful for future vdW spintronic devices.

Since the discovery of graphene,[1)] studies of two-dimensional atomic crystals have been actively conducted.[2)] Layered materials enable fabrication of atomically-thin films using the mechanical exfoliation technique, retaining the quality of bulk crystal structure. Thus, these materials are expected to be applied to high-purity thin film devices.[3,4)] In recent years, materials exhibiting phase transitions such as superconductivity and ferromagnetism have been fabricated into single-layer or few-layer devices.[6–19)] Among them, few-layer ferromagnets, namely van der Waals (vdW) ferromagnets, have attracted much attention in the field of spintronics because of their potential device applications.[13,15)] $Cr_2Ge_2Te_6$[11,14,19)] and CrI_3[12,13)] are semiconducting or insulating vdW ferromagnets, while Fe_3GeTe_2[15–17)] and V_5Se_8[18)] are metallic vdW ferromagnets. In spite of several candidates for vdW ferromagnets, most of these candidates have Curie temperatures T_C lower than room temperature without gating. For spintronic device applications, vdW ferromagnets with T_C higher than room temperature are highly desirable.

Fe_5GeTe_2 is a recently-reported layered-ferromagnetic metal with $T_C \approx 310$ K.[20–23)] Fe_5GeTe_2 has a similar crystal structure to Fe_3GeTe_2 but with additional Fe atoms as shown in Fig. 1(a). It is known that Fe_3GeTe_2 exhibits a strong perpendicular magnetic anisotropy (PMA) in bulk form, and the amplitude of the magnetization monotonically increases with decreasing temperature.[17,24–26)] On the other hand, the magnetic state in Fe_5GeTe_2 is much more complex than Fe_3GeTe_2. The magnetization in Fe_5GeTe_2 increases with decreasing temperature as in Fe_3GeTe_2, but it takes a maximum at around 120 K and start to decrease as the temperature decreases.[22)] Unlike Fe_3GeTe_2, Fe_5GeTe_2 does not exhibit a PMA in bulk form, while the PMA has been reported in thin film devices.[21)] In addition, according to the X-ray diffraction measurement,[22)] Fe_5GeTe_2 has a structural phase transition at 550 K. Thus, the crystal structure depends on how the crystal is cooled down. When Fe_5GeTe_2 is immediately cooled down after its growth in a furnace at around 1000 K, which is referred to as "quenched" (Q) sample, the diffraction pattern is shaper than that of non-quenched (NQ) sample, indicating a better crystal quality. Although Fe_5GeTe_2 has many interesting physical properties, details of the PMA in thin films are still largely unclear, and further research is vital for future vdW spintronic device applications.

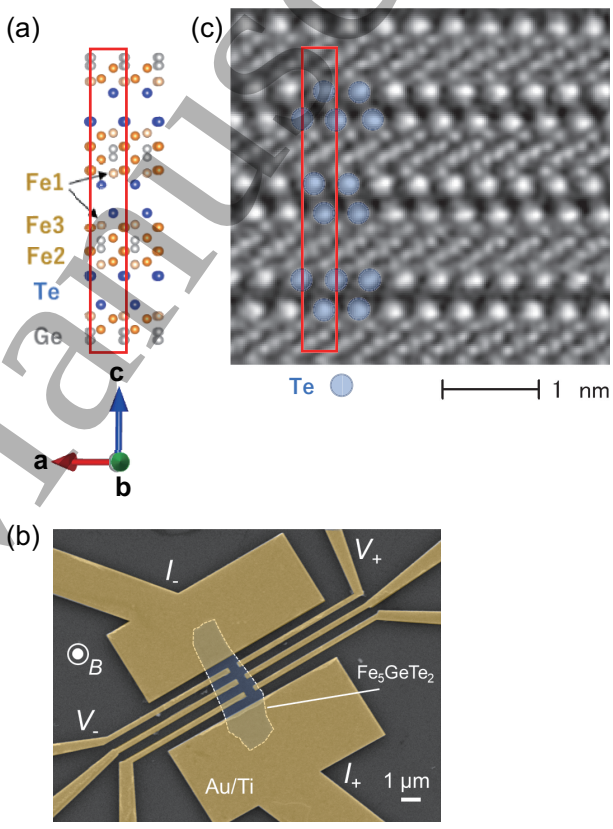

Fig. 1. (a) Schematic of crystal structure of Fe_5GeTe_2. The red square corresponds to the unit-cell of Fe_5GeTe_2. (b) SEM image of one of the Fe_5GeTe_2 thin film devices. The electrode configuration for the Hall measurement is added in the image. (c) TEM image of the 18L NQ-Fe_5GeTe_2 device. The blue sphere indicates the Te atom.

In this work, we have fabricated thin film devices using Q- and NQ-Fe_5GeTe_2 samples and performed electrical transport measurements from 310 K down to 2 K. The longitudinal resistivity ρ_{xx} of Q-Fe_5GeTe_2 devices has a larger temperature dependence than that of NQ-devices.

*niimi@phys.sci.osaka-u.ac.jp

As the number (n) of the unit-cell layer (L) decreases, the resistivity change becomes larger. The Hall resistivity ρ_{yx} shows almost the same temperature dependence in both Q- and NQ-devices when n is larger than 10. ρ_{yx} increases with decreasing temperature from 310 K but starts to decrease at 100 K, below which the coercivity becomes larger. For the thinner film devices, on the other hand, a Q-device has a much larger coercive field than a NQ-device. This result originates from the difference of the crystal structures between Q- and NQ-crystals, which should yield a stronger impact in thinner films.

Single crystals of Fe_5GeTe_2 were synthesized in an evacuated quartz tube with an I_2 transport agent. The tube was heated up to 1050 K and kept at this temperature for one week. NQ-samples were obtained by letting them naturally cool down to room temperature in the quartz tube, while Q-samples were obtained by rapidly cooling down to room temperature (in practice, by dipping the tube into water). We confirmed from the X-ray diffraction pattern that both NQ- and Q-samples are single crystals, and confirmed from the energy-dispersive X-ray spectroscopy measurement that the composition ratio of Fe, Ge, and Te is 5.3, 1, and 2.4, respectively, both for NQ- and Q-samples, which hereafter we simply call Fe_5GeTe_2. The lattice constant along the a-axis is $a = 4.04$ Å both for Q-Fe_5GeTe_2 and NQ-Fe_5GeTe_2, while the lattice constant along the c-axis changes depending on the cooling process: $c = 29.19$ Å for Q-Fe_5GeTe_2 and $c = 29.04$ Å for NQ-Fe_5GeTe_2. The lattice constants are consistent with those in Ref.[21)]

To obtain thin film devices, we adopted the mechanical exfoliation technique using scotch tape. Since the thin film is easily oxidized, the exfoliation process has been performed in a globe box filled with Ar gas of purity 99.9999%. Some of the exfoliated Fe_5GeTe_2 flakes were transferred from the scotch tape to a thermally-oxidized silicon substrate. To attach electrodes to the exfoliated Fe_5GeTe_2 thin films, we performed electron beam lithography on polymethyl-methacrylate resist. After the development of the resist inside the globe box, Ti and Au were deposited in a chamber next to the globe box. The thicknesses of Ti and Au were 5 and 100 nm, respectively. Figure 1(b) shows a scanning electron microscopy (SEM) image of our typical Fe_5GeTe_2 thin film device. In order to check the quality of the exfoliated Fe_5GeTe_2 thin film, a cross sectional transmission electron microscopy (TEM) image was taken for 18L NQ-Fe_5GeTe_2 device in Fig. 1(c). We can confirm that the obtained TEM image is consistent with the crystal structure of Fe_5GeTe_2 shown in Fig. 1(a), although the Fe1 site is difficult to see in the TEM image as pointed out in Ref.[21)]

Figure 2 shows the temperature dependence of the longitudinal resistivity ρ_{xx} for Q- and NQ-Fe_5GeTe_2 devices with different numbers of L. To compare four different data, ρ_{xx} is normalized at $T = 10$ K. For all the devices, there is a large resistivity drop at around 100-120 K. This drop would be related to the magnetic ordering at the Fe1 site (see Fig. 1(a)), as mentioned in Ref.[21)] The temperature at which the resistivity drop occurs shifts to the lower side with decreasing n. In addition, the normalized resistivities of Q-devices are larger than those of

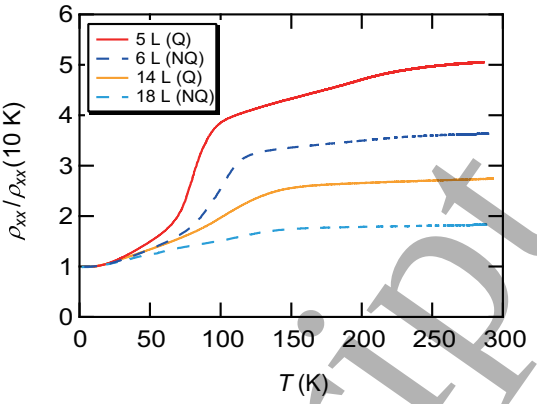

Fig. 2. Temperature dependence of the resistivity for Q- (solid lines) and NQ-Fe_5GeTe_2 (broken lines) devices with different numbers of L. The resistivity $\rho_{xx}(T)$ is normalized at $T = 10$ K. $\rho_{xx}(10\ \mathrm{K})$ is about 100 $\mu\Omega$·cm.

NQ-devices. The result suggests that the Q-devices have less defects than the NQ-devices. This is also consistent with the previous X-ray result where the diffraction intensity is shaper for bulk Q-samples.[22)]

Next, we measured the Hall resistivity ρ_{yx} for Q- and NQ-Fe_5GeTe_2 devices with different numbers of L. Figures 3(a) and 3(b) show the anomalous Hall effect obtained with thick (more than 10L) Q-Fe_5GeTe_2 and NQ-Fe_5GeTe_2 devices at two typical temperatures (50 K and 200 K). A hysteresis loop can be seen for both devices at 50 K, but the loop shape is not clearly rectangular. The coercive field H_c defined from $\rho_{yx}(H_c) = 0$ becomes smaller with increasing temperature, while the anomalous Hall resistivity (ρ_A), obtained by extrapolating the linear fit at high magnetic fields to zero field (see Fig. 3(a)), increases as the temperature is increased, and takes a maximum at around 150 K. The above tendencies can be seen more clearly in the temperature dependence of ρ_A and H_c shown in Figs. 3(c) and 3(d), respectively. T_C determined from ρ_{yx} is more than 310 K for both devices, although it is in general higher than T_C determined from magnetization measurements.[27)]

A clear difference between Q- and NQ-Fe_5GeTe_2 appears in thinner devices. In Figs. 4(a) and 4(b), we show the anomalous Hall effect obtained with 5L Q-Fe_5GeTe_2 and 6L NQ-Fe_5GeTe_2 devices at two typical temperatures (50 K and 200 K). The hysteresis loop is much closer to an ideal rectangular shape, compared to thicker films. In particular, H_c of 5L Q-Fe_5GeTe_2 is about six times larger than that of the thicker Q-Fe_5GeTe_2. This means that the PMA becomes stronger with decreasing thickness of Fe_5GeTe_2. More importantly, H_c of 5L Q-Fe_5GeTe_2 is about two times larger than that of 6L NQ-Fe_5GeTe_2 at 50 K. The difference of H_c becomes smaller with increasing temperature and disappears at around 100 K where the anomalous Hall resistivity ρ_A takes a maximum, as shown in Figs. 4(c) and 4(d). As we increase temperature further, H_c becomes zero at 230 K and ρ_A vanishes at $T_C = 295$ K, lower than thicker devices. The reduction of T_C in thinner Fe_5GeTe_2 is consistent with that of other vdW ferromagnets.[11–19)]

Now we discuss ρ_A and H_c in the low temperature

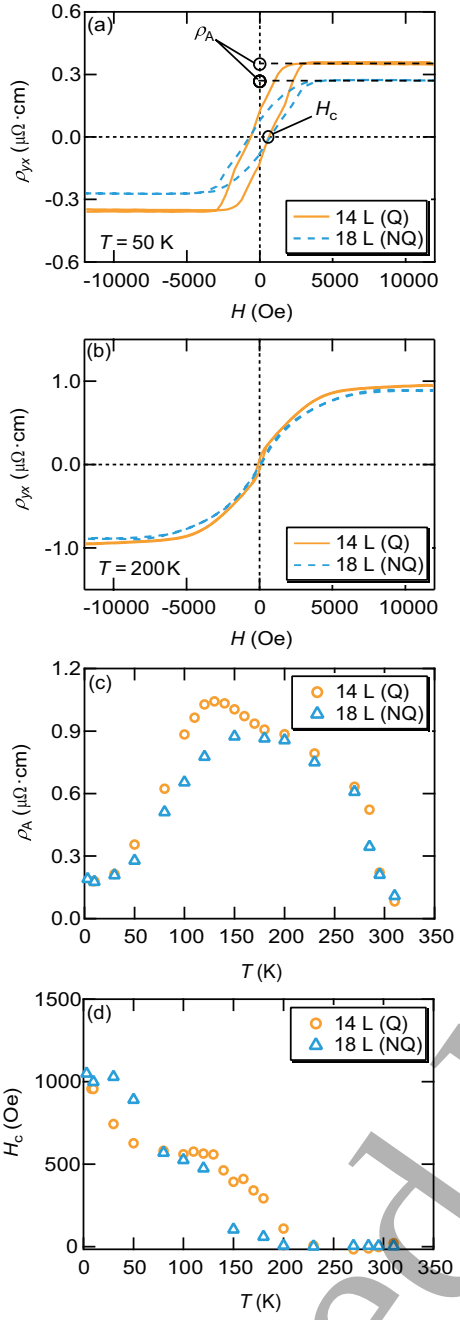

Fig. 3. Hall resistivity of thick (more than 10L) Q- and NQ-Fe_5GeTe_2 devices measured at (a) 50 K and (b) 200 K. The orange solid and light blue dashed lines are the results obtained with 14L Q-Fe_5GeTe_2 and 18L NQ-Fe_5GeTe_2 devices, respectively. ρ_A and H_c mean the anomalous Hall resistivity and the coercive field, respectively. Temperature dependence of (c) ρ_A and (d) H_c of 14L Q- and 18L NQ-Fe_5GeTe_2 devices. The orange circle and light blue triangle indicate the results of 14L NQ-Fe_5GeTe_2 and 18L NQ-Fe_5GeTe_2, respectively.

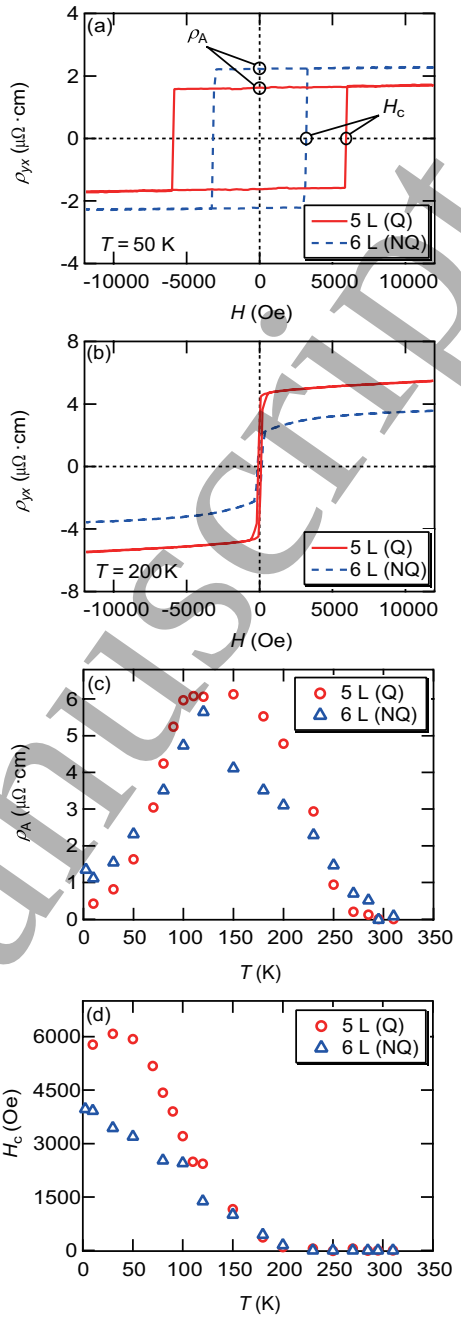

Fig. 4. Hall resistivity of thin (less than 10L) Q- and NQ-Fe_5GeTe_2 devices measured at (a) 50 K and (b) 200 K. The red solid and blue dashed lines are the results obtained with 5L Q-Fe_5GeTe_2 and 6L NQ-Fe_5GeTe_2 devices, respectively. Temperature dependence of (c) ρ_A and (d) H_c of 5L Q- and 6L NQ-Fe_5GeTe_2 devices. The red circle and blue triangle indicate the results of 5L NQ-Fe_5GeTe_2 and 6L NQ-Fe_5GeTe_2, respectively.

region. In the case of general ferromagnets, ρ_A monotonically increases with decreasing temperature, but in the present case, ρ_A takes a maximum at around 100-150 K regardless of the thickness and decreases with decreasing temperature below 100 K. It is also reported in Ref.[21] that the Fe1 site is magnetically ordered at a similar temperature ($\sim$ 120 K). From these facts, we can deduce the possibility that Fe_5GeTe_2 could be a ferrimagnet rather than a ferromagnet, unlike a simple ferromagnetic Fe_3GeTe_2.[17] As for H_c, the value becomes larger with decreasing temperature and thickness. Such a tendency can be expected for general ferromagnets because of shape magnetic anisotropy, but the atomically thin Q-Fe_5GeTe_2 device has a much larger H_c value than the NQ counterpart, although T_C and ρ_A are almost the same. According to Ref.,[22] Q-Fe_5GeTe_2 has a higher crystal symmetry than NQ-Fe_5GeTe_2. The detailed crystal structure is a crucial component in the discussion of the difference between the two results. This should be ad-

dressed in further detail through other experiments such as X-ray magnetic circular dichroism measurements and by performing the first principles calculations in near future.

In summary, we have fabricated Q- and NQ-Fe_5GeTe_2 thin film devices and performed electrical transport measurements. The normalized ρ_{xx} takes a larger value for Q-Fe_5GeTe_2 as well as thinner devices. The observed anomalous Hall resistivity has a maximum at around 100-150 K and decreases with decreasing temperature. These results suggest ferrimagnetic ordering in Fe_5GeTe_2, rather than a simple ferromagnetism. Thin Fe_5GeTe_2 devices show a stronger PMA and the coercive field monotonically increases with decreasing temperature. In addition, the 5L Q-Fe_5GeTe_2 device has coercive field two times larger than the 6L NQ-device. These differences are likely due to the detailed crystal structures of Q- and NQ-Fe_5GeTe_2 thin film samples, and further research is desired. Atomically thin Q-Fe_5GeTe_2 devices would enable us to tune not only T_C[17,28] but also the PMA[29,30] by gating, as in the case of a simple thin ferromagnetic film. These features should be useful in future vdW spintronic devices.

Acknowledgement We thank K. Kuroki, M. Ochi, H. Ishizuka, T. Kondo, K. Kuroda, K. Yamagami, and H. Wadati for fruitful discussions. We acknowledge M. Watanabe with assistance in the revision of the manuscript. The cell structure of Fe_5GeTe_2 was visualized using VESTA.[31] This work was supported by JSPS KAKENHI (Grant Numbers JP16H05964, JP17K18756, JP19K21850, JP26103002, JP19H00656, JP19H05826), Mazda Foundation, Shimadzu Science Foundation, Yazaki Memorial Foundation for Science and Technology, SCAT Foundation, Murata Science Foundation, Toyota Riken Scholar, and Kato Foundation for Promotion of Science.

1) K. S. Novoselov, A. K. Geim, S. V. Morozov, D. Jiang, Y. Zhang, S. V. Dubonos, I. V. Grigorieva, and A. A. Firsov, Science **306**, 666 (2004).
2) K. S. Novoselov, D. Jiang, F. Schedin, T. J. Booth, V. V. Khotkevich, S. V. Morozov, and A. K. Geim, Proc. Natl. Acad. Sci. USA, **102**, 10451 (2005).
3) A. K. Geim and I. V. Grigorieva, Nature 499, 419 (2013).
4) K. S. Novoselov, A. Mishchenko, A. Carvalho, and A. H. Castro Neto, Science **353**, aac9439 (2016).
5) Y. Cao, A. Mishchenko, G. L. Yu, E. Khestanova, A. P. Rooney, E. Prestat, A. V. Kretinin, P. Blake, M. B. Shalom, C. Woods, J. Chapman, G. Balakrishnan, I. V. Grigorieva, K. S. Novoselov, B. A. Piot, M. Potemski, K. Watanabe, T. Taniguchi, S. J. Haigh, A. K. Geim, and R. V. Gorbachev, Nano Lett. **15**, 4914 (2015).
6) J.-F. Ge, Z.-L. Liu, C. Liu, C.-L. Gao, D. Qian, Q.-K. Xue, Y. Liu, and J.-F. Jia, Nat. Mater. **14**, 285 (2015).
7) J. Shiogai, Y. Ito, T. Mitsuhashi, T. Nojima, and A. Tsukazaki, Nat. Phys. **12**, 42 (2016).
8) M. M. Ugeda, A. J. Bradley, Y. Zhang, S. Onishi, Y. Chen, W. Ruan, C. Ojeda-Aristizabal, H. Ryu, M. T. Edmonds, H.-Z. Tsai, A. Riss, S.-K. Mo, D. Lee, A. Zettl, Z. Hussain, Z.-X. Shen, and M. F. Crommie, Nat. Phys. **12**, 92 (2016).
9) X. Xi, Z. Wang, W. Zhao, J.-H. Park, K. T. Law, H. Berger, L. Forro, J. Shan, and K. F. Mak, Nat. Phys. **12**, 139 (2016).
10) Y. Yu, L. Ma, P. Cai, R. Zhong, C. Ye, J. Shen, G. D. Gu, X. H. Chen, and Y. Zhang, Nature **575**, 156 (2019).
11) C. Gong, L. Li, Z. Li, H. Ji, A. Stern, Y. Xia, T. Cao, W. Bao, C. Wang, Y. Wang, Z. Q. Qiu, R. J. Cava, S. G. Louie, J. Xia, X. Zhang, Nature **546**, 265 (2017).
12) B. Huang, G. Clark, E. Navarro-Moratalla, D. R. Klein, R. Cheng, K. L. Seyler, D. Zhong, E. Schmidgall, M. A. McGuire, D. H. Cobden , W. Yao, D. Xiao, P. Jarillo-Herrero, and X. Xu, Nature **546**, 270 (2017).
13) T. Song, X. Cai, M. W. Tu, X. Zhang, B. Huang, N. P. Wilson, K. L. Seyler, L. Zhu, T. Taniguchi, K. Watanabe, M. A. McGuire, D. H. Cobden, D. Xiao, W. Yao, and X. Xu, Science **360**, 1214 (2018).
14) Z. Wang, T. Zhang, M. Ding, B. Dong, Y. Li, M. Chen, X. Li, J. Huang, H. Wang, X. Zhao, Y. Li, D. Li, C. Jia, L. Sun, H. Guo, Y. Ye, D. Sun, Y. Chen, T. Yang, J. Zhang, S. Ono, Z. Han, and Z. Zhang, Nat. Nanotech. **13**, 554 (2018).
15) X. Wang, J. Tang, X. Xia, C. He, J. Zhang, Y. Liu, C. Wan, C. Fang, C. Guo, W. Yang, Y. Guang, X. Zhang, H. Xu, J. Wei, M. Liao, X. Lu, J. Feng, X. Li, Y. Peng, H. Wei, R. Yang, D. Shi, X. Zhang, Z. Han, Z. Zhang, G. Zhang, G. Yu, and X. Han, Sci. Adv. **5**, eaaw8904 (2018).
16) Z. Fei, B. Huang, P. Malinowski, W. Wang, T. Song, J. Sanchez, W. Yao, D. Xiao, X. Zhu, A. F. May, W. Wu, D. H. Cobden, J.-H. Chu, and X. Xu, Nat. Mater. **17**, 778 (2018).
17) Y. Deng, Y. Yu, Y. Song, J. Zhang, N. Z. Wang, Z. Sun, Y. Yi, Y. Z. Wu, S. Wu, J. Zhu, J. Wang, X. H. Chen, and Y. Zhang, Nature **563**, 94 (2018).
18) M. Nakano, Y. Wang, S. Yoshida, H. Matsuoka, Y. Majima, K. Ikeda, Y. Hirata, Y. Takeda, H. Wadati, Y. Kohama, Y. Ohigashi, M. Sakano, K. Ishizaka, and Y. Iwasa, Nano Lett. **19**, 8806 (2019).
19) H. Idzuchi, A. E. Llacsahuanga Allcca, X. C. Pan, K. Tanigaki, and Y. P. Chen, Appl. Phys. Lett. **115**, 232403 (2019).
20) J. Stahl, E. Shlaen, and D. Johrendt, Z. Anorg. Allg. Chem. **644**, 1923 (2018).
21) A. F. May, D. Ovchinnikov, Q. Zheng, R. Hermann, S. Calder, B. Huang, Z. Fei, Y. Liu, X. Xu, and M. A. McGuire, ACS Nano **13**, 4436 (2019).
22) A. F. May, C. A. Bridges, and M. A. McGuire, Phys. Rev. Materials **3**, 104401 (2019).
23) M. Joe, U. Yang, and C. Lee, Nano Mater. Sci. **1**, 299 (2019).
24) B. Chen, J. Yang, H. Wang, M. Imai, H. Ohta, C. Michioka, K. Yoshimura, and M. Fang, J. Phys. Soc. Jpn. **82**, 124711 (2013).
25) A. F. May, S. Calder, C. Cantoni, H. Cao, and M. A. McGuire, Phys. Rev. B **93**, 014411 (2016).
26) H. L. Zhuang, P. R. C. Kent, and R. G. Hennig, Phys. Rev. B **93**, 134407 (2016).
27) D. H. Wei, Y. Niimi, B. Gu, T. Ziman, S. Maekawa, and Y. Otani, Nat. Commun. **3**, 1058 (2012).
28) D. Chiba, S. Fukami, K. Shimamura, N. Ishiwata, K. Kobayashi, and T. Ono, Nat. Mater. **10**, 853 (2011).
29) M. Tsujikawa and T. Oda, Phys. Rev. Lett. **102**, 247203 (2009).
30) T. Seki, M. Kohda, J. Nitta, and K. Takanashi, Appl. Phys. Lett. **98**, 212505 (2011).
31) K. Momma, F. Izumi, J. Appl. Cryst. **44**, 1272-1276 (2011).